Group-index independent coupling to band engineered SOI photonic crystal waveguide with large slow-down factor

Somayyeh Rahimi,[1,3,*] Amir Hosseini,[1,3] Xiaochuan Xu,[1] Harish Subbaraman,[2] and Ray T. Chen[1]

[1]*Microelectronic Research Center, Department of Electrical and Computer Engineering, University of Texas, 10100 Burnet Rd., Austin, TX 78758, USA*
[2]*Omega Optics, Inc, 10306 Sausalito Dr., Austin, TX 78759, USA*
[3]*Joint first authors*
**nrahimi@utexas.edu*

Abstract: Group-index independent coupling to a silicon-on-insulator (SOI) based band-engineered photonic crystal (PCW) waveguide is presented. A single hole size is used for designing both the PCW coupler and the band-engineered PCW to improve fabrication yield. Efficiency of several types of PCW couplers is numerically investigated. An on-chip integrated Fourier transform spectral interferometry device is used to experimentally determine the group-index while excluding the effect of the couplers. A low-loss, low-dispersion slow light transmission over 18nm bandwidth under the silica light line with a group index of 26.5 is demonstrated, that corresponds to the largest slow-down factor of 0.31 ever demonstrated for a PCW with oxide bottom cladding.

OCIS codes: (230.7390) Waveguides, planar; (130.5296) Photonic crystal waveguides.

References and links

1. M. Soljačić, S. G. Johnson, S. H. Fan, M. Ibanescu, E. Ippen, and J. D. Joannopoulos, "Photonic-crystal slow-light enhancement of nonlinear phase sensitivity," J. Opt. Soc. Am. B **19**(9), 2052–2059 (2002).
2. R. Iliew, C. Etrich, T. Pertsch, and F. Lederer, "Slow-light enhanced collinear second-harmonic generation in two dimensional photonic crystals," Phys. Rev. B **77**(11), 115124 (2008).
3. Y. Jiang, W. Jiang, L. Gu, X. Chen, and R. T. Chen, "80-micron interaction length silicon photonic crystal waveguide modulator," Appl. Phys. Lett. **87**(22), 221105 (2005).
4. W.-C. Lai, S. Chakravarty, X. Wang, C. Lin, and R. T. Chen, "On-chip methane sensing by near-IR absorption signatures in a photonic crystal slot waveguide," Opt. Lett. **36**(6), 984–986 (2011).
5. M. Notomi, K. Yamada, A. Shinya, J. Takahashi, C. Takahashi, and I. Yokohama, "Extremely large group-velocity dispersion of line-defect waveguides in photonic crystal slabs," Phys. Rev. Lett. **87**(25), 253902 (2001).
6. H. C. Nguyen, Y. Sakai, M. Shinkawa, N. Ishikura, and T. Baba, "10 Gb/s operation of photonic crystal silicon optical modulators," Opt. Express **19**(14), 13000–13007 (2011).
7. A. Y. Petrov and M. Eich, "Zero dispersion at small group velocities in photonic crystal waveguides," Appl. Phys. Lett. **85**(21), 4866–4868 (2004).
8. J. M. Brosi, J. Leuthold, and W. G. Freude, "Microwave-frequency experiments validate optical simulation tools and demonstrate novel dispersion-tailored photonic crystal waveguides," J. Lightwave Technol. **25**(9), 2502–2510 (2007).
9. M. D. Settle, R. J. P. Engelen, M. Salib, A. Michaeli, L. Kuipers, and T. F. Krauss, "Flatband slow light in photonic crystals featuring spatial pulse compression and terahertz bandwidth," Opt. Express **15**(1), 219–226 (2007).
10. L. H. Frandsen, A. V. Lavrinenko, J. Fage-Pedersen, and P. I. Borel, "Photonic crystal waveguides with semi-slow light and tailored dispersion properties," Opt. Express **14**(20), 9444–9450 (2006).
11. S. Kubo, D. Mori, and T. Baba, "Low-group-velocity and low-dispersion slow light in photonic crystal waveguides," Opt. Lett. **32**(20), 2981–2983 (2007).
12. J. Li, T. P. White, L. O'Faolain, A. Gomez-Iglesias, and T. F. Krauss, "Systematic design of flat band slow light in photonic crystal waveguides," Opt. Express **16**(9), 6227–6232 (2008).
13. Y. Hamachi, S. Kubo, and T. Baba, "Slow light with low dispersion and nonlinear enhancement in a lattice-shifted photonic crystal waveguide," Opt. Lett. **34**(7), 1072–1074 (2009).
14. D. Mori and T. Baba, "Wideband and low dispersion slow light by chirped photonic crystal coupled waveguide," Opt. Express **13**(23), 9398–9408 (2005).

#153276 - $15.00 USD Received 22 Aug 2011; revised 4 Oct 2011; accepted 6 Oct 2011; published 20 Oct 2011

15. Y.-S. Chen, Y. Zhao, A. Hosseini, D. Kwong, W. Jiang, S. R. Bank, E. Tutuc, and R. T. Chen, "Delay time enhanced flat band photonic crystal waveguides with capsule-shaped holes on silicon nanomembrane," IEEE J. Sel. Top. Quantum Electron. **15**(5), 1510–1514 (2009).
16. M. Notomi, A. Shinya, K. Yamada, J. Takahashi, C. Takahashi, and I. Yokohama, "Structural tuning of guiding modes of line defect waveguides of silicon on insulator photonic crystal slabs," IEEE J. Quantum Electron. **38**(7), 736 (2002).
17. M. G. Scullion, T. F. Krauss, and A. Di Falco, "High efficiency interference for coupling into slotted photonic crystal waveguide," IEEE Photonics J. **3**(2), 203–208 (2011).
18. R. Hao, E. Cassan, X. Le Roux, D. Gao, V. Do Khanh, L. Vivien, D. Marris-Morini, and X. Zhang, "Improvement of delay-bandwidth product in photonic crystal slow-light waveguides," Opt. Express **18**(16), 16309–16319 (2010).
19. A. Hosseini, X. Xu, D. N. Kwong, H. Subbaraman, W. Jiang, and R. T. Chen, "On the role of evanescent modes and group index tapering in slow light photonic crystal waveguide coupling efficiency," Appl. Phys. Lett. **98**(3), 031107 (2011).
20. A. Gomez-Iglesias, D. O'Brien, L. O'Faolain, A. Miller, and T. F. Krauss, "Direct measurements of the group index of photonic crystal waveguide via Fourier transform spectral interferometry," Appl. Phys. Lett. **90**(26), 261107 (2007).
21. S. A. Schulz, L. O'Faolain, D. M. Beggs, T. P. White, A. Melloni, and T. F. Krauss, "Dispersion engineered slow light in photonic crystals: a comparison," J. Opt. **12**(10), 104004 (2010).
22. J. Nocedal and S. Wright, *Numerical Optimization* (Springer-Verlag, 1999).
23. S. G. Johnson, P. Bienstman, M. A. Skorobogatiy, M. Ibanescu, E. Lidorikis, and J. D. Joannopoulos, "Adiabatic theorem and continuous coupled-mode theory for efficient taper transitions in photonic crystals," Phys. Rev. E Stat. Nonlin. Soft Matter Phys. **66**(6), 066608 (2002).
24. P. Pottier, M. Gnan, and R. M. De La Rue, "Efficient coupling into slow-light photonic crystal channel guides using photonic crystal tapers," Opt. Express **15**(11), 6569–6575 (2007).
25. C.-Y. Lin, X. Wang, S. Chakravarty, B. S. Lee, W.-C. Lai, and R. T. Chen, "Wideband group velocity independent coupling into slow light silicon photonic crystal waveguide," Appl. Phys. Lett. **97**(18), 183302 (2010).
26. J. P. Hugonin, P. Lalanne, T. P. White, and T. F. Krauss, "Coupling into slow-mode photonic crystal waveguides," Opt. Lett. **32**(18), 2638–2640 (2007).
27. N. Ozaki, Y. Kitagawa, Y. Takata, N. Ikeda, Y. Watanabe, A. Mizutani, Y. Sugimoto, and K. Asakawa, "High transmission recovery of slow light in a photonic crystal waveguide using a hetero groupvelocity waveguide," Opt. Express **15**(13), 7974–7983 (2007).
28. C. Martijn de Sterke, K. B. Dossou, T. P. White, L. C. Botten, and R. C. McPhedran, "Efficient coupling into slow light photonic crystal waveguide without transition region: role of evanescent modes," Opt. Express **17**(20), 17338–17343 (2009).
29. Y. Cui, K. Liu, D. L. MacFarlane, and J. B. Lee, "Thermo-optically tunable silicon photonic crystal light modulator," Opt. Lett. **35**(21), 3613–3615 (2010).
30. Y. A. Vlasov and S. J. McNab, "Coupling into the slow light mode in slab-type photonic crystal waveguides," Opt. Lett. **31**(1), 50–52 (2006).
31. R. Jacobsen, A. Lavrinenko, L. Frandsen, C. Peucheret, B. Zsigri, G. Moulin, J. Fage-Pedersen, and P. Borel, "Direct experimental and numerical determination of extremely high group indices in photonic crystal waveguides," Opt. Express **13**(20), 7861–7871 (2005).
32. W. Song, R. A. Integlia, and W. Jiang, "Slow light loss due to roughness in photonic crystal waveguides: An analytic approach," Phys. Rev. B **82**(23), 235306 (2010).

1. Introduction

The slow light effect in photonic crystal waveguides (PCW) provides a strong light-matter interaction, which enhances absorption, non-linearity and gain per unit length [1,2], with several applications ranging from low-power and compact optical modulation [3] to gas detection [4]. However, the narrow bandwidth of PCW slabs due to their highly dispersive group velocity in the slow light regime, restricts their applications [5]. As an example, a PCW Mach-Zehnder modulator operating with RF bandwidth as high as 10Gb/s was recently reported, but the optical bandwidth was only 0.7nm [6]. Therefore, in order to cover over 20nm optical bandwidth in a typical integrated dense wavelength-division multiplexing (DWDM) system, several different designs will be necessary. In order to avoid having different PCW modulators for operation at each optical wavelength, a PCW design that can achieve slow light operation over a large bandwidth is required.

Band-engineered PCWs have been shown to provide low-dispersion slow-light suitable for applications such as optical buffers and delay lines [7]. Different ways of achieving low group velocity dispersion in single PCWS have been presented including adjustments of a) the waveguide width [7–9], b) the air hole size of the first two innermost rows [10,11], c) the displacement of the first two innermost rows, and d) the displacement of the third innermost

#153276 - $15.00 USD Received 22 Aug 2011; revised 4 Oct 2011; accepted 6 Oct 2011; published 20 Oct 2011

row [12,13]. Most of the methods mentioned above have been tested for air-bridged structures [12–15]. Slow down factor (SF), which is the normalized bandwidth - group index product, as high as 0.31 has been reported for air-bridged silicon-nanomembrane based PCWs [12]. Realizing constant group velocity propagation over a wide bandwidth and with guided mode well-below the silica light line in such a SOI PCW is more challenging than in air-bridged PCWs.

Although air top and bottom claddings increase the PCW guided mode bandwidth, the SOI PCWs provides some engineering advantages compared to the air-bridged PCWs. 1) mature silicon CMOS fabrication technology tools can be used that enable PCW fabrication with sufficient accuracy [16], 2) the SOI structure facilitates fabrication of PCW devices that consist of separate silicon sections (please see Fig. 1 of [17]), 3) in general, eliminating any fabrication step (removal of the buried oxide layer) will improve the fabrication yield.

By perturbing holes adjacent to the waveguide core, the highest reported SF for a SOI PCW with bottom oxide cladding is 0.24 [10] corresponding to a group index of 34. Band engineering techniques that do not require multiple hole-sizes, such as changing the positions of the first two rows [12] or lattice-shifting [13,18], provide the advantage of higher yield and reproducibility. Among these techniques, lattice-shifting makes it easier to target a desired group velocity over a bandwidth of interest since these two parameters can be tuned relatively independently [13]. The largest SF experimentally presented by this technique is 0.19 [13].

In this paper, we present a lattice-shifting based design for low-dispersion slow-light SOI PCW. Integration of several slow-light PCW based devices requires the problem of large insertion losses due to strong impedance mismatch between strip waveguides and slow light propagation in PCW to be addressed. Thus, we also discuss different band engineering techniques from coupling efficiency point of view. A step-coupler [19] is designed to provide group-index-independent coupling into and out of the band engineered PCW. A single hole-size is used for both coupler and PCW. For an accurate measurement of group index, a complete on-chip device based on Fourier transform spectral interferometry [20] is designed and fabricated. A large SF of 0.31 and group-index-independent coupling over an 18nm bandwidth of low-dispersion slow light propagation is confirmed experimentally. Efficient optical coupling and slow-light operation over a large optical bandwidth provides a means for realization of larger optical bandwidth and high speed compact PCW based modulators. An example of such devices will be reported elsewhere.

2. Design and simulations

A schematic of the band engineered PCW is shown in Fig. 1. The lattice constant (a) is 392nm. The thickness of the silicon layer and the buried oxide layers are 250nm and 3μm, respectively. Band engineering can be done by tuning the hole sizes [10] or the positions of the rows adjacent to the line defect. However, lattice shifting is more desirable as it has proved to be a fabrication friendly approach [21], while the accurate control of several different hole sizes is a challenging task. Two different approaches of lattice shifting, longitudinal (parallel to the defect line) and lateral (perpendicular to the defect line), are shown in Fig. 1. A slow-down factor as high as 0.3 has been demonstrated for an air-bridged PCW band-engineered by lateral lattice shifting [12]. Thus far, the highest experimentally determined SF for a PCW band-engineered by longitudinal lattice shifting has been 0.19 [13]. Theoretically however, SF as large as 0.35 is estimated by longitudinal lattice shifting of the two innermost rows [18].

We perform simulations using RSoft 3D BandSolve. Figures 2(a) and 2(b) show the effect of longitudinal and lateral lattice shifting, respectively, on the band structure. An important observation is that longitudinal lattice shifting does not change the position of the fundamental PCW defect mode in the fast light region. In the case of lateral lattice shifting, for a large SF value, a large positive value of t_1 is necessary [12] that effectively increases the defect line width (dW) and thus causes red shift in the defect mode band. Therefore, for our design, we choose the longitudinal lattice shifting of the first three rows on the two sides of

#153276 - $15.00 USD Received 22 Aug 2011; revised 4 Oct 2011; accepted 6 Oct 2011; published 20 Oct 2011

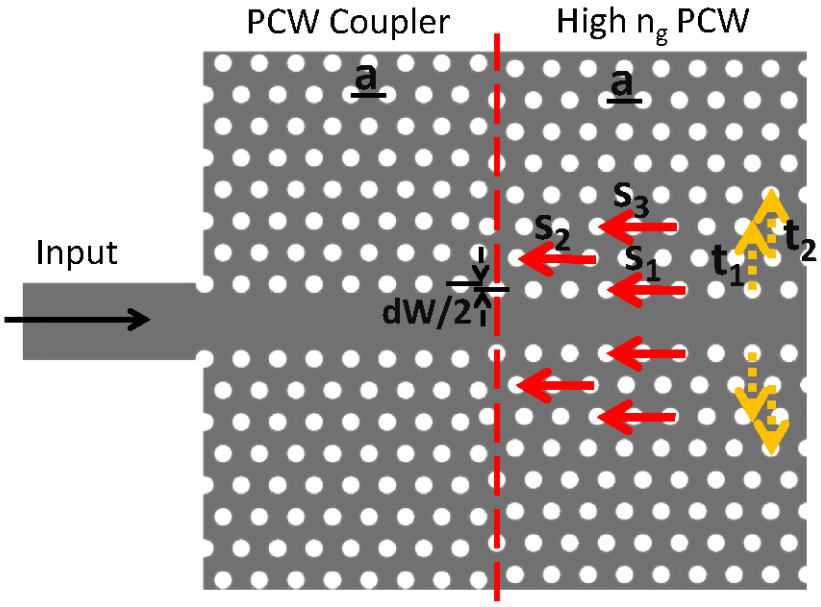

Fig. 1. Schematic of band engineered PCW and PCW taper. Longitudinal (parallel to the defect line) and lateral (perpendicular to the defect line) lattice shifting are depicted by red (solid) and yellow (dashed) arrows, respectively. The directions of the arrows indicate the positive direction assumed in this paper.

the defect line. As will be discussed later, this choice also facilitates the design of the input/output coupler. For design optimization process, we utilize sequential quadratic programming (SQP), a nonlinear programming technique that exploits the gradients of the objective and constraint functions at each iteration to accelerate convergence [22]. The independent variables are s_1, s_2, s_3 and r, where s_i (i = 1, 2, 3) represents the amount of lateral shifting for the i^{th} row of air holes, and r is the hole radius. Similar to the results presented in [18], we find that a large longitudinal shift of the innermost rows results in a minimum in the defect mode dispersion curve below the silica light line and at normalized k<0.5 [Fig. 2(a)]. Although the resulting SF can be large, using FDTD we find that coupling into the desired section of the defect mode band in such PCWs is inefficient (typically, maximum normalized transmission <15%). In contrast, in the case of band engineered PCWs with their defect mode minimum at the band-edge (k = 0.5), normalized transmission over the low-dispersion bandwidth can reach 50% without use of any couplers [Fig. 2(d)]. Therefore, another constraint in the optimization process is to keep the defect mode minimum at the band-edge. Figure 2(c) shows the band structure of the designed band-engineered low-dispersion slow light PCW (r = 0.27a, s_1 = 0, s_2 = –0.05a and s_3 = 0.25a) with n_g = 26.7 ± 10% over a bandwidth of 18nm corresponding to SF of 0.31. Note that the second and third rows are shifted in opposite directions.

An important consideration for practical applications is efficient coupling into the slow-light region from an access ridge waveguide. Coupling efficiency can be improved by inserting a group index taper [23–25] or a fast light PCW region between the access ridge waveguide and the PCW [12,19,26,27]. In principle, the performance (transmission efficiency) of the group index tapers scale badly with increasing group index [21]. The existence of evanescent modes at the interface of a fast light PCW and a slow light PCW helps satisfy the boundary conditions [19,28] thus improve coupling efficiency. Numerical and experimental investigations reveal that a step coupler, which is a special implementation for the fast light PCW region, outperforms group index tapers realized by the defect mode

#153276 - $15.00 USD Received 22 Aug 2011; revised 4 Oct 2011; accepted 6 Oct 2011; published 20 Oct 2011

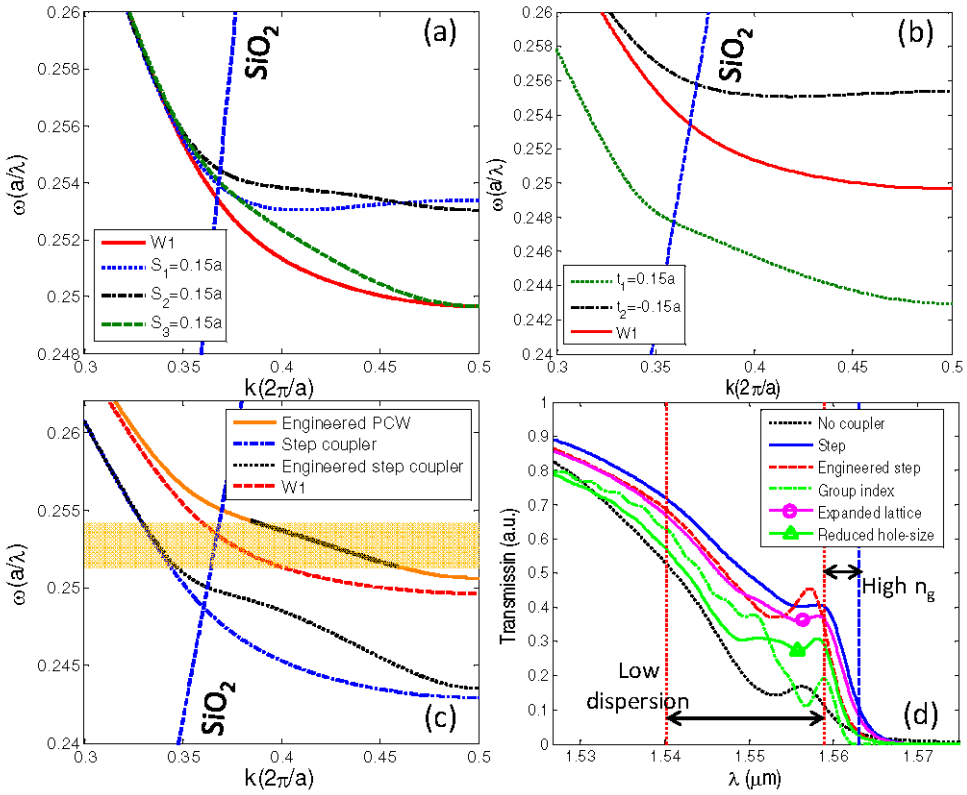

Fig. 2. PWC band structures with (a) 0.15a longitudinal lattice shifting, (b) 0.15a lateral lattice shifting. For each defect mode curve, at most only one lattice row (on each side of the line defect) is shifted. (c) Band structures of the designed band-engineered PCW, dW = 0, s_1 = 0, s_2 = –0.05a, s_3 = 0.25a, step coupler (r = 0.27a, dW = 0.15a, s_1 = s_2 = s_3 = 0), and an engineered step coupler (r = 0.27a, dW = 0.15a, s_1 = 0, s_2 = –0.05a, s_3 = 0.25a). The low-dispersion bandwidth is highlighted by a black line on the defect mode of the designed band-engineered PCW. (d) FDTD simulations of a single interface between different fast-light PCW and the designed band-engineered PCW. Vertical dashed line indicates the band-edge of the designed PCW defect mode. Vertical dotted lines indicate the boundaries of the low-dispersion bandwidth. Step coupler, Engineered step, Expanded lattice, Reduced hole-size couplers refer to (a = 392nm, r = 0.27a, dW = 0.15a, s_1 = s_2 = s_3 = 0), (a = 392nm, r = 0.27a, dW = 0.15a, s_1 = 0, s_2 = –0.05a, s_3 = 0.25a), (a = 420nm, r = 0.27a, dW = 0, s_1 = s_2 = s_3 = 0), and (a = 392nm, r = 0.23a, dW = 0.15a, s_1 = s_2 = s_3 = 0), respectively. In the case of the group index taper, the hole sizes of a W1 PCW (a = 392nm, r = 0.27a, dW = 0.0a, s_1 = s_2 = s_3 = 0) at the interface with the slow light PCW are parabolically reduced to r = 0.23a at the interface with the ridge waveguide. In all cases, the coupler (or taper) length is 8 periods.

width modulation [19]. In comparison to the slow light PCW, a fast light PCW coupler defect mode is red-shifted so that the steep section of its defect mode overlaps with the desired bandwidth of the slow light PCW. This can be realized in different ways, such as reducing the hole sizes while retaining the original lattice constant [27], expanding the hole spacing while retaining the same hole size [21], and increasing the defect mode width (also known as the step coupler) while retaining all the other parameters the same [19].

The step coupler presented in [19] was designed for efficient coupling into a W1 PCW. An increase in the defect line width red-shifts the defect mode band, and consequently, its low-group index bandwidth overlaps with the bandwidth of interest. Three-dimensional FDTD simulations show that increasing the defect line width more than about 0.15a-0.20a results in diminishing returns [19]. However, a question to be answered is whether the fast light PCW designed to couple light into band engineered PCW should itself be band

#153276 - $15.00 USD Received 22 Aug 2011; revised 4 Oct 2011; accepted 6 Oct 2011; published 20 Oct 2011

engineered. In other words, how must the values of s_1, s_2 and s_3 be chosen? Figure 2(c) shows the band structures of a non-engineered PCW step coupler (r = 0.27a, dW = 0.15a, $s_1 = s_2 = s_3 = 0$) and an engineered PCW step coupler (r = 0.27a, dW = 0.15a, $s_1 = 0$, $s_2 = -0.05$a and $s_3 = 0.25$a). One notices that the non-engineered coupler has a more consistent efficiency inside the low-dispersion bandwidth. Another important observation is that in the case of a step coupler, the usable part of the band lies slightly above the silica light line. However, both numerical and experimental results show that the silica bottom cladding does cause negligible radiation loss for a small number of periods (less than 16) [19]. The same phenomenon was also observed in the case of the group index tapers [25]. We believe that as long as the holes are not filled with silica, the effective light line lies between that of air and silica, and specifically, the radiation loss can be ignored for small number of periods.

In order to numerically investigate the efficiencies of different couplers, we simulate transmission through a structure consisting of a ridge silicon waveguide, 8 periods of a fast light region, and 13 periods of the designed band-engineered PCW (dW = 0, $s_1 = 0$, $s_2 = -0.05$a and $s_3 = 0.25$a) using RSoft 3D FDTD. Note that step couplers with longer than 8 periods do not further improve the transmission efficiency for group indices lower than 30 [19]. The length of the slow light section is chosen to be 13 periods so that the transmission spectrum becomes independent from the number of periods.

For the sake of comparison, we also simulate a structure only consisting of a ridge silicon waveguide and 13 periods of the designed band-engineered PCW with no coupler. Figure 2(d) compares the normalized transmission of several different couplers against the case in which no coupler is used. Couplers (or fast light PCWs) include *Step coupler* (r = 0.27a, dW = 0.15a, $s_1 = s_2 = s_3 = 0$), *Engineered Step coupler* (r = 0.27a, dW = 0.15a, $s_1 = 0$, $s_2 = -0.05$a and $s_3 = 0.25$a), *Group Index Taper* (dW = 0, $s_1 = s_2 = s_3 = 0$), where the hole radii are gradually decreased (quadratically) from the interface of the engineered PCW with the fast light PCW to the interface of fast light PCW with the ridge waveguide by 15nm [25], *Expanded Lattice coupler* in which the hole spacing in the fast light region is increased by 30nm (see Fig. 5 of [21]), and finally, *Reduced Hole-size* coupler (r = 0.24a, dW = 0.15a, $s_1 = s_2 = s_3 = 0$), in which the holes sizes are about 10nm smaller in radius compared to the engineered PCW [27].

Only *Step coupler* and *Expanded Lattice coupler* result in complete designs with a single hole size. As demonstrated in Fig. 2(d), the *Step coupler* outperforms all the other types in the bandwidth of interest. Figure 2(d) also indicates that the *Engineered Step coupler* provides the sharpest transition near the band edge, and thus it is a good candidate for devices such as band-edge cut-off based modulators [29].

Here, we notice an advantage of longitudinal lattice shifting compared to lateral lattice shifting in designing the coupler region. When linearizing the defect mode band by lateral lattice shifting, the defect mode of the fast light PCW is red-shifted compared to that of the slow-light PCW. Since longitudinal lattice shifting does not red-shift the defect mode, designing the coupler requires less widening of the defect line and also the wider photonic band gap is expected from the experimental results. We find that using the step coupler design, the best coupling into the designed engineered PCW is at least 4% more efficient over the low-dispersion bandwidth compared to coupling into a laterally shifted lattice design (dW = 0, r = 0.295a, $t_1 = 0.15$a, and $t_2 = 0$) with nearly similar SF = 0.28 and $n_g = 25.5$. Our final device consists of 250 periods of the designed band engineered PCW (r = 0.27a, dW = 0, $s_1 = 0$, $s_2 = -0.05$a and $s_3 = 0.25$a) and 8 periods of the Step coupler (r = 0.27a, dW = 0.15a, $s_1 = s_2 = s_3 = 0$) on each side.

In the case of SOI PCWs, the useful optical bandwidths of the step coupler, engineered step coupler, group index taper and the reduced hole-size coupler all lay near but above the Silica light line. However, based on the FDTD simulation results as long and the couplers are short [here all couplers are 8 periods (3.14μm) long], the propagation loss inside the couplers due to optical coupling to substrate radiation modes is negligible. Therefore, for the same designs we expect that the same conclusions hold true if the PCWs are air-bridged.

For an accurate measurement of group index, an integrated on chip device, which works based on Fourier transform spectral interferometry [20] is also designed and fabricated.

#153276 - $15.00 USD Received 22 Aug 2011; revised 4 Oct 2011; accepted 6 Oct 2011; published 20 Oct 2011

Compared to the other group-index measurement techniques, such as detecting Fabry-Perot interference inside the sample itself [30] or time of flight measurements [31], this method provides group index as a function of wavelength over the transmission band in a single-shot measurement and without uncertainty in choosing the fringes' maxima [20]. The scheme presented herein integrates delay lines, beam splitters and beam combiners on the same chip as the PCW device and also eliminates post-sample polarization compared to the Mach-Zehnder interferometric setup presented in [20].

3. Fabrication and test setup

The chip is fabricated on commercially available SOI wafers from SOITEC, which have a 250nm thick silicon device layer, 3μm thick buried oxide (BOX) layer and a 500μm thick silicon handle substrate layer. After electron beam lithography (JEOL JBX-6000) and developing, the resist pattern is transferred to the silicon layer using an HBr/Cl_2 RIE etch. A microscope image of the fabricated chip is shown in Fig. 3.

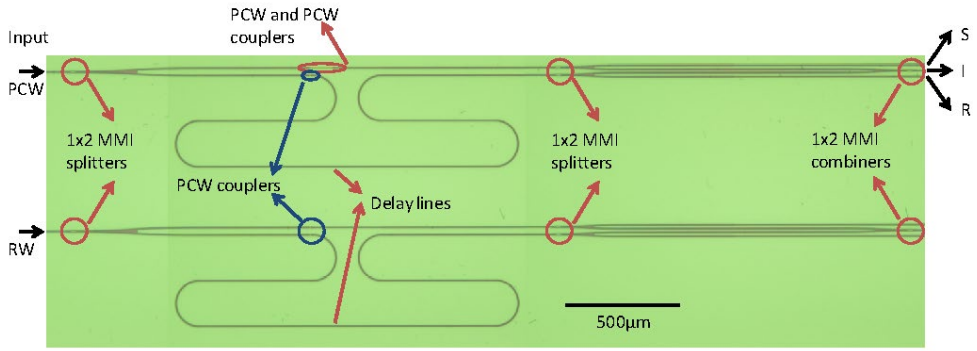

Fig. 3. A microscope image of the fabricated on-chip group index measurement device. The top device contains the PCW and PCW couplers in one arm of the Mach-Zehnder structure and a delay line and PCW couplers in the other arm. In the bottom device, the PCW is replaced with a ridge waveguide.

A scanning electron microscope (SEM) picture of the fabricated PCW device is shown in Fig. 4. The red dashed line shown in Fig. 4(a) demarcates the high n_g PCW from the specially engineered PCW step coupler. The purpose of the step coupler, as discussed in Section 2, is to provide efficient light coupling from a silicon strip waveguide into the high n_g PCW device. A zoomed-in SEM image of the PCW air holes is shown in Fig. 4(b).

In order to test the device, light from a broadband amplified spontaneous emission (ASE) source, covering 1520–1620 nm, was Transverse Electric (TE)-polarized with an extinction ratio of over 30dB and butt coupled through a polarization maintaining (PM) fiber into each of the two devices shown in Fig. 3. In the top device, the input power is then uniformly divided into two arms of a Mach-Zehnder structure using a 1x2 multimode interference coupler (MMI) shown in Fig. 4(c). One arm (Signal) in the MZ is down tapered and connected to the band-engineered PCW with input/output step couplers. The other arm (Reference) in the MZ is down tapered and connected to 16 periods of the step coupler (combining the input 8 period and output 8 period couplers with no band-engineered PCW). Following the step coupler in the reference arm is a long delay waveguide with length > 5mm, which is needed for phase calculations. The reason for including the PCW couplers is to enhance transmission though the device and to suppress Fabry-Perot oscillations between highly reflective interfaces. Both the Signal and Reference arms are connected to 1x2 MMIs to provide 2 samples of each signal (S and R). One output from each of these MMIs is combined to provide the Interference signal (I). The bottom device is similar to the top one with this difference that the engineered PCW is replaced with a ridge silicon waveguide. The bottom device is required for normalize the test results and explained in Section 4.

#153276 - $15.00 USD Received 22 Aug 2011; revised 4 Oct 2011; accepted 6 Oct 2011; published 20 Oct 2011

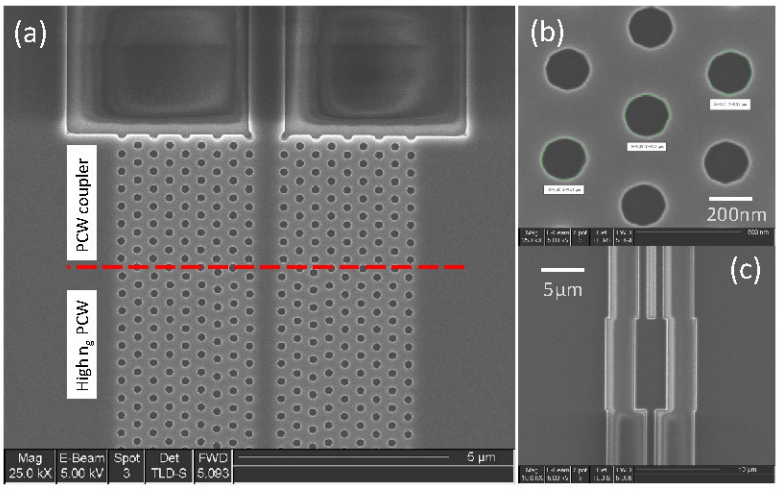

Fig. 4. (a) SEM pictures of the fabricated PCW device showing the PCW coupler and high n_g region, (b) close up of the PCW air holes, (c) 1x2 MMI device employed for splitting and merging the signal coming from two arms of MZI device.

4. Analysis and discussions of test results

The mathematical approach to map the group index of the dispersion profile is given in [20]. For the sake of completeness, we summarize the technique as follows. The interference (I) spectral intensity from any of the two arms is given as

$$I(\omega) = S(\omega) + R(\omega) + \sqrt{S(\omega)R(\omega)}\exp(i\varphi(\omega) - i\omega\tau) + c.c. \quad (1)$$

where S(ω) and R(ω) are the spectral intensity outputs of the Signal (S) and Reference (R) arm, respectively, and τ is the time delay from the delay line. φ(ω) is the phase difference between S and I, and therefore, contains the group index data. In order to calculate the group index, the complex interference term is extracted from I by numerically filtering the signal peak with a peck at τ in the time domain. The result is then Fourier transformed back into frequency domain from which the phase data, $\varphi(\omega) - \omega\tau$, is extracted. Based on the phase data, the group delay of the top device containing the device under test (PCW), $\Delta T^{PCW} = d(\varphi(\omega) - \omega\tau)/d\omega$ is calculated. Applying the same technique on the signals measured from the bottom device, the group delay (ΔT^{RW}) is obtained. Finally, the group index from the PCW is calculated from the difference between the calculated group delays from the two devices, given as

$$n_g(\omega) = (\Delta T^{PCW}(\omega) - \Delta T^{RW}(\omega))c/L + n^{RW}(\omega) \quad (2)$$

where L is the engineered PCW without the couplers and n^{RW} (from RSoft FEMSim simulations) is effective index of the ridge waveguide replacing the engineered PCW in the bottom device. In order to increase the accuracy of the measurement we also include the input/output PCW couplers in Mach-Zehnder setup. However, their effect on the group index measurement is cancelled out because the PCW couplers are included in both arms of both devices.

The measured I, S (the same as PCW transmission), and R signals for our device are shown in Fig. 5(a), where the measured spectrums are vertically shifted for better visibility. Note that our choice for the length of reference arm is made so that the slowing of light in the PCW arm decreases the difference in group delay between the two arms, thus leading to an increase in fringe spacing. Figure 5(b) shows the calculated group index as a function of wavelength based on the experimental data. Our results indicate a low-dispersion (with less

#153276 - $15.00 USD Received 22 Aug 2011; revised 4 Oct 2011; accepted 6 Oct 2011; published 20 Oct 2011

than ±10% fluctuations in group index) transmission over 18 nm bandwidth with an average group index of 26.5.

We note that backscattering loss (induced by side wall roughness), which is the dominant factor for n_g>10, scales with n_g^2 in PCWs [32]. The relatively constant measured transmission not only over the low-dispersion slow light bandwidth (1539nm-1556nm), but also at shorter wavelength (λ<1539nm) that corresponds to smaller group indices, is due to small length of the PCW compared to the ridge waveguide. The TE propagation loss in a fabricated 500nm x 230nm waveguide is estimated using a cutback technique and is determined to be 7.3dB/cm at λ = 1550. Similar observation was made before in [12], where for a band-engineered PCW designed for n_g~30 over the low-dispersion bandwidth (similar to our PCW), group-index independent transmission was observed over the low-dispersion band width and the fast light region (n_g<<30). However, for the band-engineered PCWs designed for n_g>35 over the low-dispersion bandwidth, a clear group-index dependent transmission was observed.

In order to estimate the device insertion loss we measure transmission through two waveguides D and N. Waveguide D includes 1) 1mm long width taper [2.5μm (matched to the lensed fiber mode size) to 0.5μm wide], about 4mm long single mode waveguide (0.5μm wide), 0.5mm long width taper [0.5μm to 0.738μm (matched to the PCW step coupler width)], 2.17μm long step PCW input step coupler, 100μm band engineered PCW, 2.17μm long step PCW output coupler, 0.5mm long width taper (0.738μm to 0.5μm), 4mm long straight single mode waveguide (0.5μm wide), and 1mm long (0.5μm to 2.5μm wide]. Waveguide N is the same as waveguide D, but the PCW step couplers and the band engineered PCW waveguides are entirely replaced by a 0.738μm wide straight ridge waveguide. All the waveguides are 230nm high. We normalized the transmission through waveguide D with regard to waveguide N to cancel out 1) input/output fiber-ridge waveguide coupling loss, 2) propagation loss in the silicon ridge waveguide, 3) taper losses. Our results indicate that the insertion loss over the low dispersion bandwidth (1539nm–1557nm) is 3.8 ± 1.1dB, which only includes input/output ridge waveguide-PCW coupling loss and propagation loss inside the PCW.

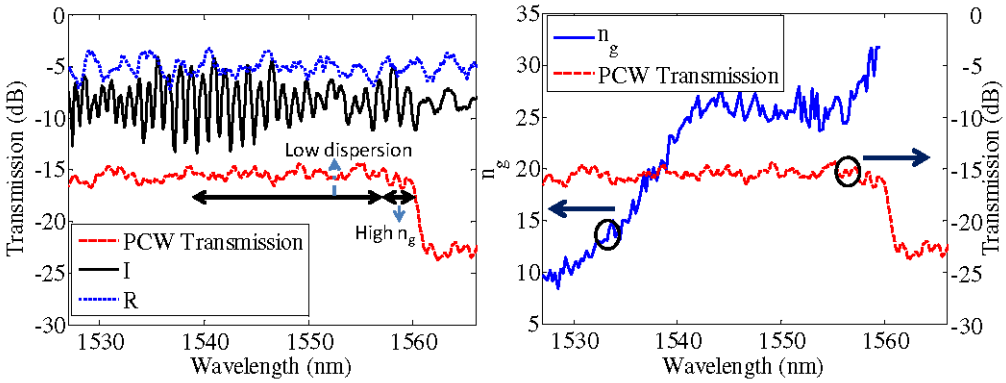

Fig. 5. (a) Output spectrum of PCW device (red curve), ridge waveguide (blue curve) and their interference (black curve). (b) Output spectrum of PCW device (red curve) and the calculated group index based on FT method (blue curve). The PCW transmission curve is also provided as a reference.

5. Conclusion

In conclusion, we presented the design of a low-loss, low dispersion and high group index photonic crystal waveguide with large slow down factor of 0.31. In order to improve coupling to the PCW, a step coupler with just one hole-size was numerically investigated and found to be more efficient over other different types of couplers. For enabling accurate on-chip group index measurement of the PCW, a scaled-down Fourier transform spectral interferometer on

#153276 - $15.00 USD Received 22 Aug 2011; revised 4 Oct 2011; accepted 6 Oct 2011; published 20 Oct 2011

SOI was also designed and fabricated for the first time. The test results indicated an average group index of 26.5 over 18nm bandwidth under the silica light line that corresponds to the largest slow-down factor of 0.31 ever reported for a PCW with oxide bottom cladding.

Acknowledgments

This research was supported by AFOSR Small Business Technology Transfer (STTR) under Grant No. FA9550-11-C-0014 (Program Manager, Dr. Gernot Pomrenke).

#153276 - $15.00 USD Received 22 Aug 2011; revised 4 Oct 2011; accepted 6 Oct 2011; published 20 Oct 2011